Communications in a Cave Environment

William Walsh
Jet Propulsion Laboratory,
California Institute of Technology
4800 Oak Grove Dr.
Pasadena, CA 91109
818-354-1681
William.B.Walsh@jpl.nasa.gov

Jay Gao
Jet Propulsion Laboratory,
California Institute of Technology
4800 Oak Grove Dr.
Pasadena, CA 91109
818-354- 9528
Jay.L.Gao@jpl.nasa.gov

Abstract— **Lava tubes are thought to exist on Mars and on the Moon, and are of special interest for science objectives and human habitability. The communications environment in such a cave is important for exploration.**

This paper explores the use of the shooting and bouncing rays (SBR) approximation to modeling the electromagnetics environment in a basalt rock lava tube with an obstruction, such as a cave-in. The cave, which has smooth walls, widens until the obstruction occurs, and then narrows. There is no line-of-sight communications path. A cave length of 100 meters is modeled. Existing knowledge of tunnel communications and the ANSYS Savant tool are leveraged in order to provide results for the cave geometry.

A number of observations are offered in the following areas based on indications obtained from lava tube modeling: (1) Enhanced signals are observed. This is the degree to which the cave walls can create an amplification of the received signal and assist communications by reflecting the incident and re-scattered signals. Communications behind the obstacle is possible. (2) Spatial signal fading was observed, hinting at geometric effects or that scattered signals can combine destructively. Deep fades occur but appear to be rare. (3) Diminished signal strength occurs at the boundaries. Robotic exploration may take place close to the cave floor or walls. Indications from simulation for signal strengths close to the cave floor and walls are examined. (4) Frequency-selective fading can occur. The time-delay spread is discussed.

The simulation results include an evaluation of IEEE 802.11 WiFi at 2.4 GHz using a freestanding electric cross dipole antenna and transmitted signal powers from 10mW to 100mW. Receive data rates are derived at locations throughout the cave and are provided to the degree that the cave geometry and electromagnetics approximations hold. These are only estimates of actual data rates subject to the approximations that were applied. Simplifications and adaptations of the WiFi waveform are discussed as part of a power trade.

TABLE OF CONTENTS

1. INTRODUCTION

Features linked to lava tubes, such as patterns of "skylights," have been visually identified on Mars and on the Moon [1]. Robotic exploration, which could provide the next level of insight, will have to communicate in the electromagnetic environment of the lava tube.

Lava tubes are thought to exist on Mars and on the Moon, and are of special interest for science objectives and human habitability. The communications environment in such a cave is important for exploration. This paper investigates the electromagnetic properties of the cave environment and how to plan a communications network, with a focus on identifying communications hazards and their workarounds. The waveform selection and optimizations for a power-constrained environment are also significant.

Using lava tubes on earth as a surrogate for those on Mars and the Moon [2], the following geometric properties are of interest. Specifically, lava tubes that

1) Are nominally a few meters across and may curve to the right or left,

2) Gain or shrink in diameter,

3) Feature obstacles such as blockage, or

4) Exhibit up/down or side passages (braided tubes), nominally obscured from line of sight.

Figure 1 shows the lava tube studied in this paper. Lava tubes are made of basalt, and the electromagnetic properties of basalt were used in these studies. The electric permittivity of basalt is taken to be constant value of ε=8.2-0.7j across the radio frequencies of interest. The magnetic permeability appears to be site specific. Simulations involving μ=1 and μ=100 were explored without significant differences in results.[1] Since finite conductivity appeared to be dependent on terrestrial humidity/dampness, the value was not considered in these studies.

[1] Non-linear hysteresis effects are not modeled

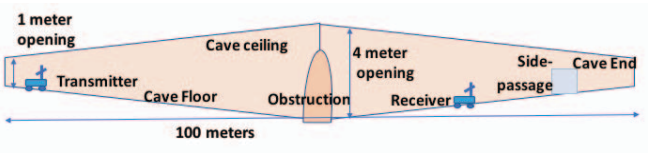

Figure 1: Overview of lava tube of interest

2. BACKGROUND

The feasibility of using WiFi at 2.4 GHz in caves has been successfully explored in field studies as recently as April this year [3].

Significant work has been done on the modeling of the electromagnetic environment of tunnels [4]. These models loosely give the following conceptual picture. When close to the transmitter and far from the walls, the signal can be described by simple space loss. Farther out, measured and simulated data are often curve-fitted to an exponential attenuation, with discussions of the tunnel acting like a waveguide. For example, in Hrovat et al. [5], an attenuation possibly in the 0.1 dB/m range might be suggested in a 500 m long, 4 m wide, 5 m high railway tunnel at 400 MHz. Prior use of ray tracing[4] is motivation that the ray tracing approach, upon which the simulations in this paper are based, can describe relevant aspects of the field present in a cave. Direct application of the two-slope tunnel model to the Martian and Lunar caves has been studied [6], which left questions about how roughness, obstructions, and narrowing or widening passageways or side passages might affect communications.

Rays are represented by flux tubes that conserve energy, including taking into account the divergence factor associated with the curvature of the wall at the prior reflection. The divergence factor is a method for accounting for spatial thinning (or focusing) of the scattered field. However, energy is lost to the refracted component of the ray into the cave wall. This refracted component depends on the electromagnetic properties of the cave walls and the angle of incidence. For shallow angles of incidence, almost all of the power is reflected, whereas for steep angles of incidence, the majority of the incident power is absorbed.

The calculation of the fields inside the cave do not use the rays directly. The rays are replaced with equivalent currents on the cave walls, and these, together with the incident field, are used in a standard integral to calculate the fields within the cave.

The geometry calculations are based on a three-dimensional cave model. The cave surface is represented by facets in formats such as the STeroLithography (STL) file format.

The results in this paper are derived using the ANSYS Savant tool [8]. The models are setup and visualized in Savant. Modern computing power and the commercial availability of multi-core optimized implementations of the SBR allow the simplified cave environments depicted to be simulated within hours to days. We made use of a computer that has a CPU with 32 cores and a GPU with thousands of cores. It should be noted that the intended use of the tool employed in this study is described as modeling antenna-antenna coupling, installed antenna gain patterns, and

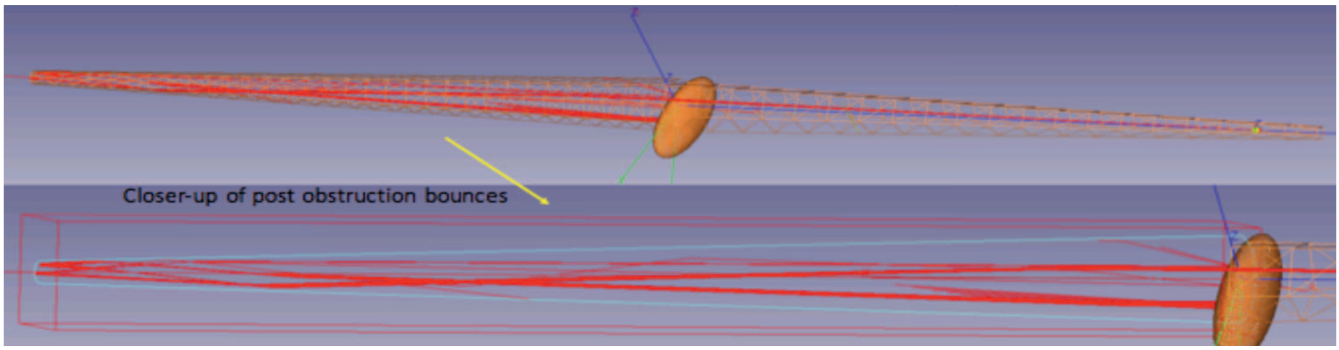

Figure 2: Example of a small set of shooting and bouncing rays in a 100 meter cave with obstruction, as visualized by Savant™

Based on the encouraging comparison between ray tracing and empirical measurements in the tunnel setting [4], the effects of the geometric shape differences are investigated in this paper using the SBR approximation.

The SBR approach [7] emanates rays from the source and derives subsequent sets of ray bounces from the cave walls based on geometric considerations. A visualization of the SBR approach is shown in Figure 2. The figure features the cave, modeled together with a limited set of rays cast to aid understanding of the SBR approach. The maximum number of bounces traced from the initial ray is a simulation parameter.

nearfields for antennas installed on electrically large platforms, typically such as ships or planes. So using it in an enclosed cave environment cannot be assumed to be well aligned with the tool optimizations or the SBR approximation, and the results are only as good as the approximations hold. Our objective is only to look for a rough model of the cave and discuss fairly generic electromagnetic phenomena.

The following features of the Savant tool are noteworthy. Savant is able to calculate a divergence factor correction by simulating the curvature of the faceted 3D surface. Savant provides options on modeling obstructions and lets the

modeler choose the degree to which geometric optics blockage or physical optics cancellations in shadowed regions is to be used.

To correlate the results being obtained by the SBR approximation with prior measurements, a simulation was performed on a somewhat analogous 500 m long tunnel of basalt walls with the transmitter 1 m off the ground. Figure 3 (top) shows the nearfield in the tunnel as depicted on cross-sectional screens spaced in ~50 m intervals. The transmitter is at the top right. It was found that, going down the tunnel, significant vertical variations in flux appeared periodic with the screen spacing. This would suggest a periodic variation of received signal strength indicator (RSSI), measured 1 meter off the floor. A 0.05 dB per meter attenuation of the signal is assessed by calculating the total energy flux[2] through the screens as shown in Figure 3. It is worth noting that after 300 meters, and with a five-bounce limit, the plot deviates from the constant attenuation per meter model. Using 20 bounces corrects this deviation, as also suggested in Hrovat et al. [4] since the increasingly shallow angles allow more reflections to contribute. The flux of incident energy through the screens is also shown. It can be seen that the re-scattered field—energy that would have dispersed into space but is captured by the cave walls in a waveguide-like effect—can account for almost an order of magnitude increase in total energy flux over the incident energy flux.

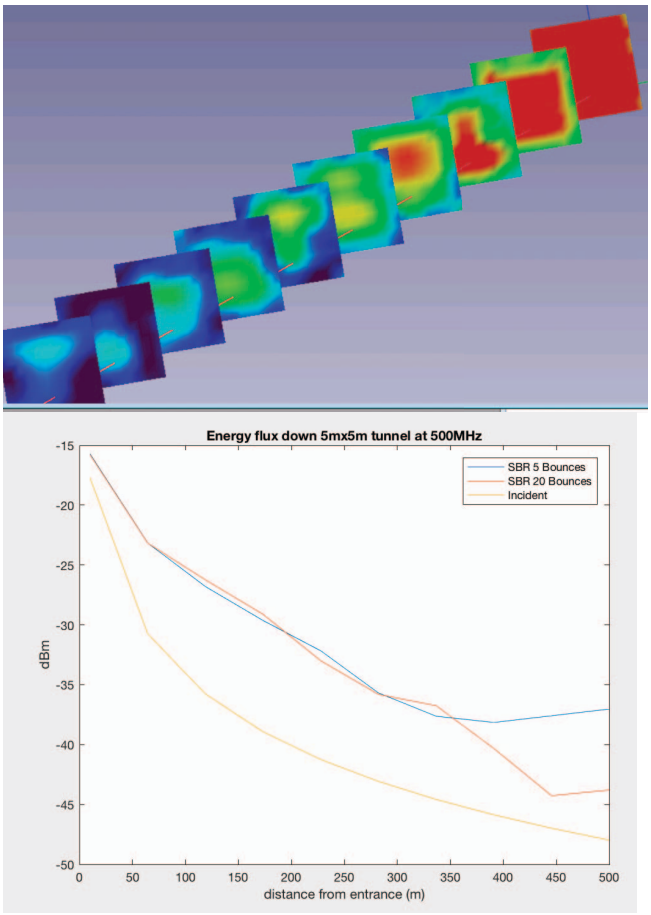

Figure 3: Energy flux in a 500 meter tunnel shown on cross sectional screens and visualized by Savant™

3. CAVE PHENOMENA

Figure 4 gives the simulation results for our chosen cave, and is the basis of the communications performance discussed in this study. The color on the screens reflects the signal strength in dB, and for contrast, the energy flux density on screen 6 is shown in linear units. Although a strong signal appears high in the cave traversing the obstruction, below, backscatter weakens the forward flux that is ultimately absorbed by the obstruction. Communications directly behind the obstruction is possible due to re-scattering of the signal. As shown in Figure 5, the average energy flux calculated in the obscured half of the cave only drops to a little less than one-half the average energy flux ahead of the obstruction. The simulation suggests that the predominant effect post-obstruction is the concentration of the energy flux as the passage narrows. Although the rise in total energy flux suggests limitation in simulation accuracies, the total energy flux does not significantly attenuate until the cave gets fairly narrow.

[2] The Poynting vector $\langle \mathbf{S} \rangle = \mathrm{re}\{\mathbf{E}_{rms} \times \mathbf{H}_{rms}^*\}$. The total flux of $\langle \mathbf{S} \rangle$ through a cave cross sectional screen - called the energy flux from now on -- is given by the area times the average S_x.

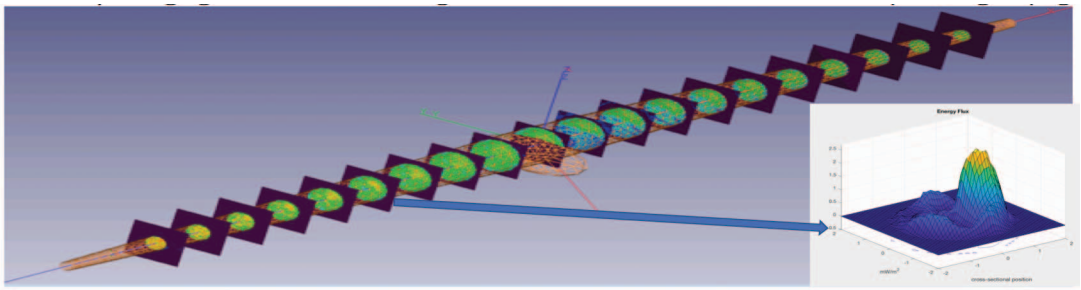

Figure 4: Results from cave simulation

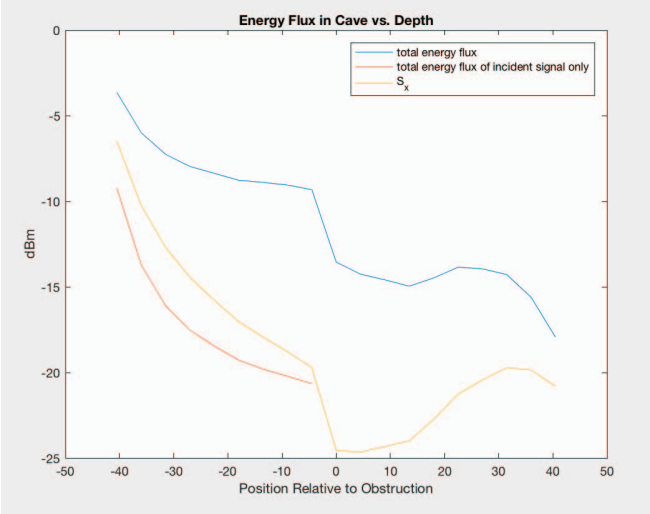

Figure 5: Total and incident energy flux across Figure 4 screens and transverse component of the Poynting vector in dB(mW/m^2)

We will examine (1) the communications environment in the five meters behind the obstruction, (2) the communications environment about 18 meters ahead of the obstruction, (3) the signal near the cave walls, and (4) the signal seeping into a side passage blocked from view at the back of the cave.

Modeling obstructions

In the case where a line-of-sight signal is not present due to an obstruction, the diffracted field around the obstruction is by default modeled by summing the incident field (post-obstruction) with the scattering field produced by the equivalent surface currents painted on the obstruction. This is consistent with the physical optics (PO) approach described earlier to compute field strength after the rays have been calculated and discarded from the computation. To compute the diffracted field, the obstruction needs to be well illuminated, as appears to be the case from the incident signal. However, Figure 5 suggests that re-scattering accounts for the majority of this signal blocked by the obstruction. These re-scattered signals blocked by the obstruction may not have optimal conditions and therefore result in simulation inaccuracies that are worse that omitting the diffracted field. To trade-off these effects, the Savant tool allows the modeler to select between PO models for an obstruction and geometric models of blockage (GO blockage). When selecting the GO blockage, the transition from PO to GO blockage calculations can be set to a user selected bounce, n ("GOn"). For example, if n=1, the incident wave cancellation post-obstruction should still use the PO model, whereas re-scattered signals should use the GO model.

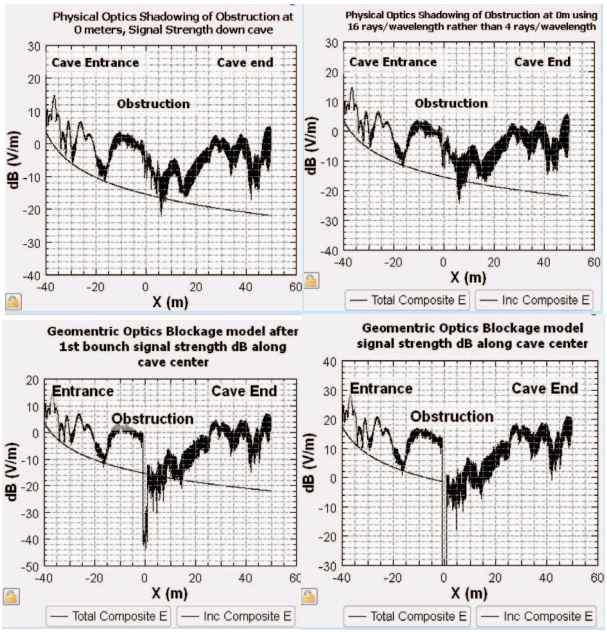

Figure 6: Field strength down center of cave as obtained via simulation using various blockage modeling options

Figure 6 provides the comparison of the signal post-obstruction simulated using PO, PO with increased ray density, GO1 and GO0. In both PO simulations, a substantial field is computed within the obstruction. Since GO1 correctly produces the expected results and employs a method that calculates the cancellation of the incident field behind the obstruction, this suggests the problem is indeed with the re-scattered fields only. The field post-obstruction does not appear different between the GO1 and GO0 simulations. This suggests that due to the large size of the obstruction, it more likely to result in re-scattering rather than diffraction at the chosen frequency.

The results in this paper make use of the GO1 approach.

Signal directly behind the obstruction

Examining the signal behind the obstruction, Figure 7 shows the square of the total electric field (in dB V/m) as a function of height above the cave floor. Although the signal levels drop by an additional factor of 100 (20 dB lower) directly behind the obstruction, it is important to keep in mind that this is relative to a signal that is still 4 times stronger than would normally be received from the transmitter 45 meters away. This suggests that traditional WiFi communications should still be possible. Since this is a scattering problem, the simulation solutions are only applicable to the specific geometry simulated.

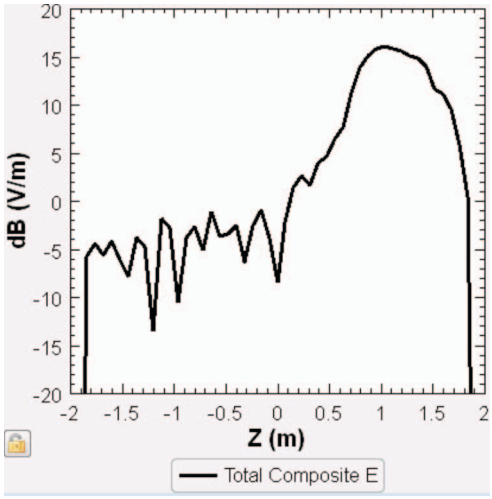

Figure 7: Field strength in the shadowed region. Communications are possible behind a large obstruction

Fading effects while in line of sight of transmitter

Taking a closer look at the signal at the screen 18 meters ahead of the obstruction, and plotting the signal in decibels (Figure 8) does reveal deep fades (blue dots). Luckily, these appear to be rare and far apart.

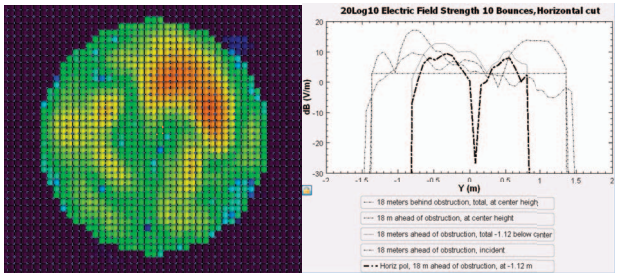

Figure 8: Field strength measurements 18 meters ahead of the obstruction showing deep fades

Ironically, despite the waveguide nature of a cave, simulation suggests that it is possible to have weak signals in front of an obstruction in full line of sight to the transmitter. Figure 9a is a simplified model showing the concept of a signal reflected from a cave wall interfering destructively with the transmitted signal. The circularly polarized freestanding resonant cross dipole antenna transmitter is facing the wall. The main aspect of the setup is the parabolic focusing effect of the wall. Looking from the wall, the signal is focused at a region about 3.5 m before reaching the transmitter, resulting in exceptionally high signal levels. As one continues toward the transmitter, the diverging signal weakens until it thins out to a point where it is at the same level in strength as the incident signal. At this point, the interference fringing, which is spatially happening over wavelength distances, can become very large. Just over 2.5 meters from the transmitter, a fade 30 dB worse than the free space link budget occurs for the case where the receiver is only able to receive the horizontal component of the circularly polarized transmission (i.e., it is oriented flat), making it impossible to receive a transmitted WiFi signal. It should be pointed out that the setup only occurs at a very narrow range in separation. The phenomena is partially mitigated if the receiver is orientated differently.

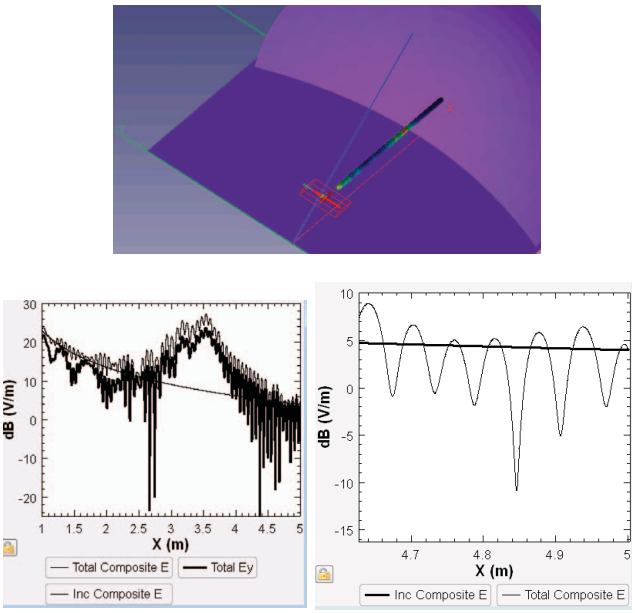

Figure 9: Spatial fading from reflected signals: (a) floor and cavern wall geometry and field strength indication, (b) signal strength between transmitter and wall, and (c) at the basalt wall

Mild spatial fading of power occurring in the couple of dB range, associated with standing waves resulting from back reflections off the obstacle or the back of the cave, is found throughout the cave. These can be seen on Figure 6. The fringing occurs over the distance of a wavelength in the electric field, and thus half a wavelength in energy flux.

Frequency selective fading

Since the fringing effect arises from the phase differences of comparable-sized signals arriving from various scatterers in the cave, the phenomena should be frequency dependent. Because the WiFi signal is transmitted with an instantaneous bandwidth of about 20 MHz, this effect could distort the transmitted signal.

Figure 10 shows the frequency-selective fading effects across the 2.4–2.5GHz WiFi band as seen 16 meters ahead of the obstruction.

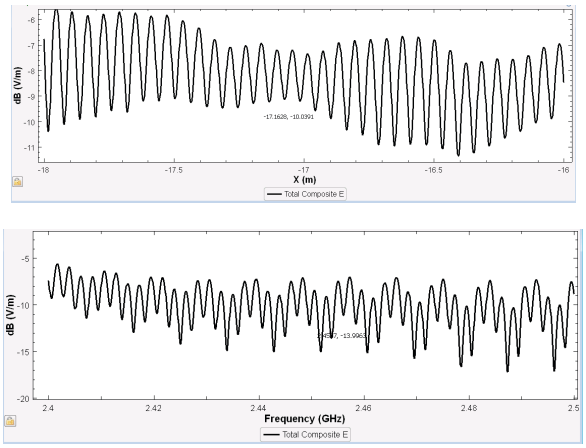

Figure 10: Signal strength 16 meters prior to obstruction: (a) Spatial fading and (b) frequency selective fading effects

The frequency-selective fading period depends on the difference in travelled distance between the interfering signals. The frequency-selective fading shown above exhibits "beats" arising from several scattered signals that can be conjectured to originate roughly 70 meters, 13 meters, and 1 meter away. These might represent the average influences of the cave end, the obstruction, and the nearby walls. The same phenomenon can be observed post-obstruction, between the cave end and the obstruction.

Cross-sectional distribution and fading

As can be seen from Figure 8, the field is not uniform across the cave cross-sectional screens and can vary by 15 dB in signal strength over 0.5 meters. On most screens shown in Figure 4, the majority of the energy flux is contained in one or a few concentrations. To get an understanding of WiFi coverage, one must recognize that the mean Poynting vector transverse component plotted in Figure 5 will largely reflect the high signal values at each screen, and that the signal is spatially distributed with areas of signal that are 10 to 15 dB weaker. This is a significant distribution, on the order of, or more significant than, the energy flux variation in the cave front to back as shown in Figure 4.

Signal close to walls

The signal will be diminished at the cave walls. Although basalt rock is luckily not a conductor, the boundary conditions do call for a reduced field. From the simulation, Figure 8 (18 meters ahead, center height, total and incident) suggests that the reduced signal at the cave walls is at least that of the equivalent incident signal level. The effects of the boundary conditions may also not be felt as much at a distance of a few wavelengths away. Figure 9 shows the boundary condition at the basalt wall. The signal often concentrates not far from the wall, when the ray reflection angles are shallow, although this is not guaranteed. The wavelength of the WiFi band at 2.4 GHz is 12.5 cm. A typical exploration rover may support an antenna height above the cave floor in excess of this number.

Side passages

Figure 11 shows how the side passage was modeled. An absorber was placed over a 1 meter by 1 meter square segment toward the backend of the cave. This segment is obscured from sight because it sits behind the obstruction and is at an obtuse angle, hiding the opening. In the simulation, the field was measured across a plane inward of the absorber, and the energy flux across the plane was taken. The simulation indicated a total of -50dB[3] of the transmitter power conveyed through the 1 m^2 opening. Similarly allocating 10dB to the side passage entrance loss, and comparing to Figure 4, this suggests that 1/1000 of the available energy flux density in the surrounding cave area may conveyed into the side passage by scattering.

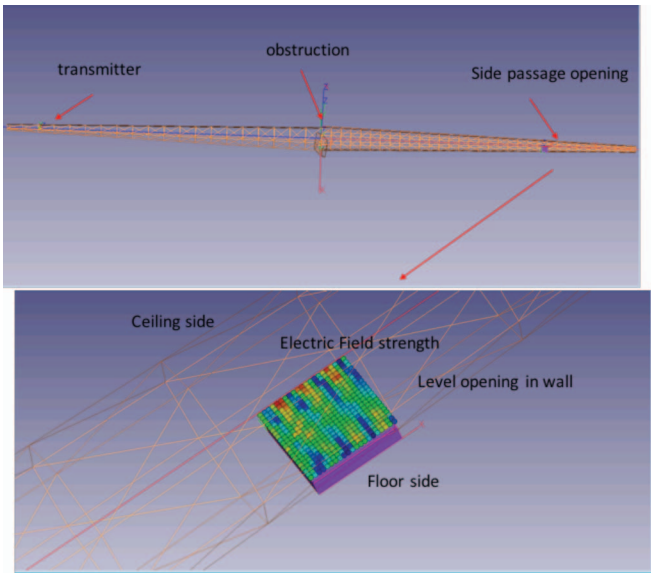

Figure 11: Method for estimating signal scattering into hidden side passage

[3] At 100mW transmit power and 10dB cave entrance loss allocation, this corresponds to -40dBm through the 1 meter[2] opening

3. USE OF 802.11 WIFI

The 802.11 OFDM waveform is specifically designed to deal with frequency-selective fading environments as identified in section 2. In section 2, the biggest time delay spread appeared be 250 ns (70 meter path difference) without any evidence of a wider spread. This is significantly smaller than the 802.11 OFDM symbol period of ~3 μs. For this reason, WiFi performance in the cave being modeled is estimated based on signal to noise rather than having to consider the inclusion of residual interference (C/I) effects of highly delayed signal energy.

In a terrestrial setting, regulation limits the transmitted power to below 100mW. Antenna and cave entrance losses were budgeted at 10 dB. These losses represent any combinations of unmodeled exploration vehicle boundary conditions, poor antenna orientation or deployment, poorer coupling into the cave than simulated, antenna loading and suboptimal voltage standing wave ratio (VSWR). The freestanding cross-dipole antenna is assumed to be optimally oriented and points toward the cave entrance.

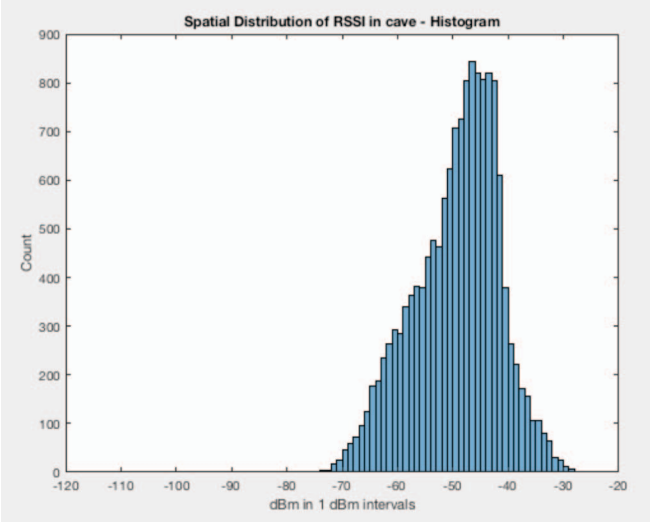

Figure 12: Distribution of WiFi RSSI encountered throughout the cave

The waveguide nature of the cave and the relative close proximity of 100 meters imply that, even with an obstruction, WiFi coverage (RSSI > -81dBm) is available. The maximum 54 Mbps rate is experienced in the majority of the cave, and locations with weaker signals are covered with reduced WiFi rates. Figure 12 shows a -44 dBm mean RSSI throughout the cave with 2.5 percent distributed below -66 dBm. This suggests a spatial fading margin of roughly 22 dB relative to the mean signal level in the cave. This margin can be suballocated to (1) fading margin within any cross section of the cave due to concentration of signal power in strong reflections, (2) signal energy flux loss due to the obstacle, (3) reduced signal level in shadowed regions, (4) attenuation by lossy cave walls, and (5) fading as a result of backscatter. Each of the quantities can be assessed based on the specific cave encountered.

Lava tubes do exhibit rough surfaces, and a simulation with surface variations up to 10 cm suggested an attenuation closer to 0.2dB/m. If 15 dB are booked for losses due to rough surfaces, the distribution suggests that communications are still possible in 97.5% of the cave.

With the exception of side passages, if the signal is lost, the spatial distributions shown from the simulations suggests that mobility would allow regaining communications.

If exploration is to include side passages, transmit power can be increased since the regulatory requirement would not apply. However, if the option is available, a mission capable of placing a relay is a more reliable approach.

Finally, it is noted that signal processing power, not transmit power, may be a limiting factor in a power-constrained environment, and especially if older technology is deployed to counter the space environment. A much simpler waveform, where WiFi coding and OFDM processing can be traded off for higher transmit power, is possible. A simplified 802.11 waveform may be deployed along with the full waveform, and the simplified waveform could be used when mobility allows the exploration vehicle to move to locations of greater signal concentration.

4. SUMMARY

A specific basalt lava tube geometry with zero conductivity and electrically flat surfaces was simulated using the SBR approach to understand the nature of communications signal scattering in a cave environment. A good WiFi signal is obtained throughout the 100 meter cave, but it is noted that each cave geometry needs to be separately considered. The chosen geometry may be optimistic in that it captures a large amount of the transmitted energy, and provides for a lot of scattering opportunity. In addition, some limitations in applying the simulation approach chosen to the cave environment were noted.

ACKNOWLEDGMENTS

The research was carried out at the Jet Propulsion Laboratory, California Institute of Technology, under a contract with the National Aeronautical and Space Administration. The authors would like to thank the JPL R&TD effort under Jay Wyatt for funding this work, and the Wireless Applique R&TD effort under Norm Lay for providing access to the simulation tool.

REFERENCES

[1] J. Haruyama, "Skylight of Underground Lava Tube on the Moon," JAXA Institute of Space and Astronautical Science, 2010, Web site: http://www.isas.jaxa.jp/e/forefront/010/haruyama/

[2] *K. McCallister, "Lava Tubes,"* Web site: http://slideplayer.com/slide/4603547/

[3] K. Belov, "Wifi measurements in a cave," unpublished

[4] A. Hrovat, G. Kandus, and T. Javornik, "A survey of Radio Propagation Modeling for Tunnels," IEEE Communications Surveys & Tutorials, Vol. 19, No. 2 pp 648-669, Second Quarter 2014

[5] A.Hrovat, G.Kandus, and T. Javornik, "Four-slope channel model for path loss prediction in tunnels at 400 MHz," microwaves, Antennas Propagation, IET, vol. 4, no. 5, pp. 571-582,

[6] J. Gao, "Application of the two-slope model to cave exploration," unpublished

[7] H. Ling, R. Chou and S. Lee, "Shooting and Bouncing Rays: Calculating the RCS of an Arbitrary Shaped Cavity," IEEE Trans. Antennas and Propagation, Vol. 37, No. 2, pp. 194-205, Feb 1989

[8] Savant Modeling tool by ANSYS, http://www.ansys.com/-/media/Ansys/corporate/resourcelibrary/brochure/ansys-savant-brochure.pdf

BIOGRAPHY

William Walsh *holds Bachelor degrees in Physics and Math from the University of Minnesota and a Masters of Science in Physics from UCLA. At NASA he has worked on the Constellation Program for human space flight and is currently working on services for high rate optical communications (LCRD program). Outside of JPL, he has worked on system and network architectures for commercial and government space based communications systems and GPS and has been Corporate Engineer at Linquest Corporation, and an associate technical fellow at Boeing.*

Jay L. Gao *joined the Jet Propulsion Laboratory in 2001 and is currently a senior research staff in the Telecommunication Research and Architecture section. His research is focused on space-based wireless communications and networking, with emphasis on adaptive data rate, demand access, and Ka-band and optical link optimization technologies for the envisioned Interplanetary Network (IPN), the Mars Relay Network, and deep space communications. He has also been a member of the Cassini Radio Science Engineering Team since 2016. He received his Ph.D. degree in Electrical Engineering from UCLA in 2000.*